SIMULATION AND ANALYSIS OF RAILWAY SYSTEM WITH POWER FLOW CONTROL OF ASYMMETRIC LC COUPLING BRANCHES

[1]M VENKATA SIVA, [2]K. MANI
[1]M.Tech, SIDDHARTH INSTITUTE OF ENGINEERING & TECHNOLOGY, Puttur, India.
[2]Associate Professor, SIDDHARTH INSTITUTE OF ENGINEERING & TECHNOLOGY, Puttur, India.

ABSTRACT : In this paper the major problem is about power quality and excessive neutral sections of the conventional two-phase electric railway supply system, The best way for adopting railway static power conditioner (RPC) which is depend upon the single-phase supply system which is a feasible solution. Therefore to improve the reliability of RPC and cost-efficiency, a novel compensating system is defined as a asymmetric double LC-coupled railway power flow conditioner (ALC-RPFC) which is introduced in this paper. The study which indicates the comparison between the proposed ALC-RPFC and the conventional RPC which have the effective heavy-load compensating ability with the lower power rating, there is more benefit to improve the converter's operating reliability and efficiency. Therefore the design technique for the LC coupling branches which is developed in this paper which is more suitable for fluctuated railway loads, and which is also used for the implemention of industrial applications. The simulation result demonstrate the good heavy-load compensating performance and power capacity reduce the ability of the ALC-RPFC.

Index Terms—Asymmetric LC-coupling branches, electrical railway power system, parameter design, power capacity analysis, power flow control.

INTRODUCTION

Considering the efficiency, adoption of the phase rotation technique is the most conventional method for electrical railway power system. However, it lacks flexibility and cannot solve all power quality problems. Moreover, these problems will become more prominent in the remote areas with unrobust power system (e.g., mountainous and plateaus areas).Compared to conventional transformers, the balance traction transformer (BTT) can have a better ability of suppressing NSC.

Unfortunately, the ability of BTT to suppress NSC is affected by load variation. Therefore, the three-phase power system can hardly be balanced by this method. Besides, this class of special-type transformer usually contains a complex winding structure, and it is also not beneficial for the elimination of harmonics and reactive power. SCR-controlled static VAR compensator can also be used to compensate NSC and reactive power in traction supply systems. But it is difficult to get a satisfactory state in both technical and economic aspects.

Compared to conventional transformers, the balance traction transformer (BTT) can have a better ability of suppressing NSC. Unfortunately, the ability of BTT to suppress NSC is affected by load variation. That is to say, the greater imbalance of two-phase loads, the worse ability of NSC suppression. Therefore, the three-phase power system can hardly be balanced by this method. Besides, this class of special-type transformer usually contains a complex winding structure, and it is also not beneficial for the elimination of harmonics and reactive power.

SCR-controlled static VAR compensator can also be used to compensate NSC and reactive power in traction supply systems. But it is difficult to get a satisfactory state in both technical and economic aspects. To overcome the disadvantages, various IGBT- or IGCT based active compensating systems were put forward in the last 20 years. Among them, RPC gets more attention due to its universalness. It can deal with almost all power quality problems of two-phase and single-phase traction supply system. However, a relatively high compensation capacity and initial investment slow down its large-scale industrial application.

TOPOLOGY OF ALC-RPFC SYSTEM

Fig. 1 shows the topology of ALC-RPFC system. The three phase 110 kV (or 220 kV) high voltage grid is stepped down into 27.5-kV single-phase traction network by Tα so as to feed locomotives.

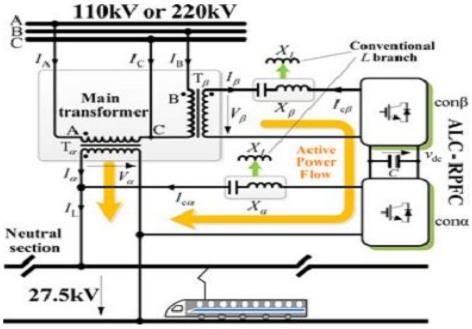

Fig. 1. Topology of ALC-RFPC system.

Fig. 2 shows the equivalent circuit of phase-α and β. Among which, Vck and Ick are the fundamental voltage and current of converter k, respectively; Xk is the equivalent fundamental reactance and VX k the voltage drop of coupling

branch in phase k, respectively; Vk and Ik are the secondary voltage and current of Tk ; IL is the load's current (k ∈ {α,β}).

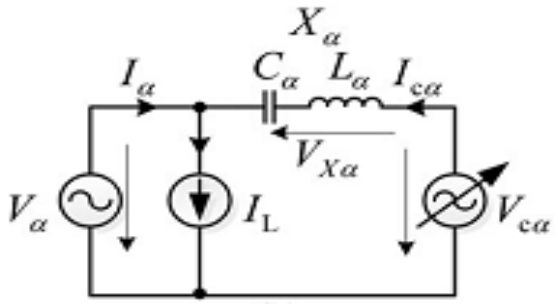

(a)

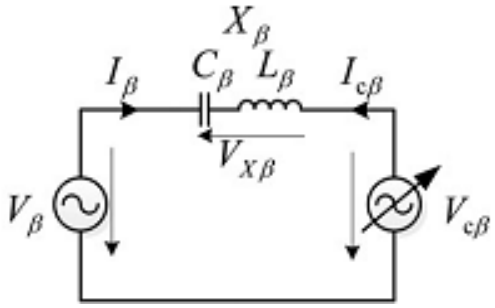

(b)

Fig. 2. Equivalent circuits of phase-α and β. (a) Phase-α. (b) Phase-β

OPERATING PROPERTY OF ALC-RPFC

Basic Requirements of Converters

Ignoring the influences of harmonics and turn's ratio difference between T α with Tβ ; the phasor diagram of ALC-RPFC is shown in Fig. 3 (Note that the voltages and currents of phase-β shown in Fig. 3 are converted to the same level of phase-α.). ALC-RPFC should satisfy the following requirements [7]:

1) Transforming half of the load's active power from phase-β (EO, i.e., 0.5ILp) to phase-α (GD, i.e., 0.5ILp).

2) Compensating appropriate leading reactive power for phase-α (BC) and lagging reactive power for phase-β (EF).

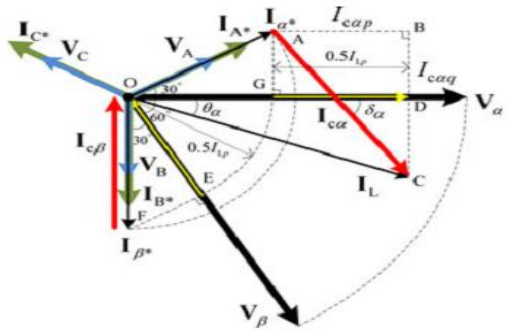

Fig. 3. Compensating phasor diagram of ALC-RPFC system.

Therefore, it can be observed from Fig. 3 that the output currents of T α and Tβ are converted from IL and 0 into Iα∗ and I β ∗, respectively. The primary three phase currents IA∗, IB∗, and IC∗ inducted by Iα∗ and Iβ ∗ are balanced as well. Obviously, their PF is 1. Hence, the compensation currents of conα and conβ are Icα and Icβ , respectively. By the way, this compensating principle is also useful for RPC [17].

To get the requirements stated previously, referring to Fig. 3, δ α(δα = ∠Vα−∠Icα) and the load's PF, λ(λ = cosθα), should satisfy

$$\delta_\alpha = arctan\left(\frac{|I_{c\alpha q}|}{|I_{c\alpha p}|}\right) = arctan\left(\frac{1}{\sqrt{3}} + 2\sqrt{\frac{1}{\lambda^2} - 1}\right) \quad (1)$$

where I cαp and Icαq are the active and reactive part of Icα, respectively (i.e., AB and BC in Fig. 3). From (1), the relationship of δ α and λ can be obtained as shown in Fig. 4.

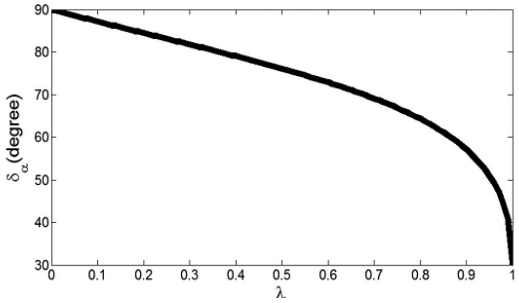

Fig. 4. Curves of δα (λ).

Obviously, δα is in inverse proportion to λ. Besides, the compensating current Icα of con α and load current IL should satisfy (2), i.e

$$I_{c\alpha} = I_{c\alpha p}^2 + I_{c\alpha q}^2 = \varepsilon I_L \quad (2)$$

where

$$\varepsilon = \sqrt{-\frac{2}{3}\lambda^2 + \frac{\lambda}{\sqrt{3}}\sqrt{1-\lambda^2} + 1} \quad (3)$$

Output Voltage of Conα

From Fig. 2(a), conα's fundamental output voltage, Vcα, can be expressed as

$$V_{c\alpha} = V_\alpha + jX_\alpha I_{c\alpha} = f(V_\alpha, X_\alpha, I_{c\alpha}, \delta_\alpha) \quad (4)$$

where X α = ωLα − 1/ωCα is the LC branch's fundamental reactance of phase-α; δα is the phase difference between Vα and I cα; f(∗) represents a function of Vα, Xα, Icα, and δα.

For an electric railway supply system, the normal voltage of Vα is a constant, while Xα will be discussed in the next section.

Situation 1: The phase of Icα is constant (i.e., δα unchanging), but its amplitude variable. Fig. 5 shows the phasor diagram of conα's output voltage (Xα < 0) when δα is constant. It can be seen from Fig. 5 that the terminal point of Vcα shifts in the vertical line of Icα(Vcα1 → V cαm → Vcα2) when Icα varies along with L2(Icα1 → Icα → I cα2). The minimum value of Vcα, Vcαm , precisely appears in the intersection point of L1 and L2 (i.e., point D).

$$\begin{cases} V_{cam} = V_\alpha \cos\delta_\alpha \\ |X_{am}| = \frac{1}{\omega C_\alpha} - \omega L_\alpha = \frac{V_\alpha \sin\delta_\alpha}{I_{c\alpha}} \end{cases} \quad (5)$$

where X αm is the LC branch's fundamental reactance of phase- α when V cα = Vcαm . Because δ α ∈ [30◦,90◦] (see Fig. 4), it can be calculated from (5) that Vcαm ∈ [0,0.866Vα]. That is to say, no matter the changes of Icα's phasor angle, Vcαm is always less than Vα, and its maximum value is only 0.866Vα.

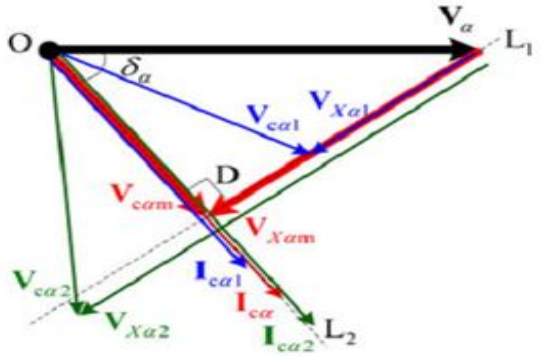

Fig. 5. Phasor diagram of conα when δα is constant.

1) Situation 2: The amplitude of Icα is constant, but its phase variable (i.e., δα variable). Fig. 6 shows the phasor diagram of conα when Icα is a constant (Xα = Xαm < 0). The variables shown in Fig. 6 satisfy the following relationship:

$$\begin{cases} I'_{c\alpha} = I_{cam} = I_{ca} \\ V'_{X\alpha} = V_{Xam} = V_{Xa} \\ \delta'_\alpha > \delta_{am} > \delta_a \\ V'_{c\alpha} = V_{cam} = V_{ca} \end{cases} \quad (6)$$

It can be seen from Fig. 6 that the smaller the phase angle between V α with the compensating current (i.e., δα < δαm < δ α'), the larger the output voltage of conα (i.e., Vcα > Vcαm > V cα').

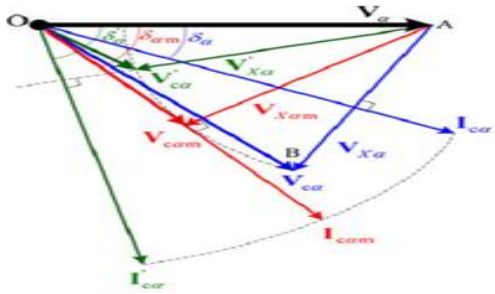

Fig. 6. Phasor diagram of conα when Icα is constant.

PARAMETER DESIGN AND SYSTEM CONTROL BASED ON THE FLUCTUATED LOAD CONDITION

Parameter Design of Phase-α

1) Synergetic Design Principle Between Xα With Conα:

It can be deduced from the previous discussions that Xα is a key parameter of ALC-RPFC, which has significant influence for the output performance of the power conditioner. To give an optimal balance between compensating performance and cost efficiency, we will give a synergetic design guideline for Xα and conα:

a) When the traction supply system operates in the heavy load situation, the output voltage of conα should be as low as possible. It allows ALC-RPFC to get the satisfactory heavy-load compensating ability with lower voltage rating and switching frequency.

b) In the premise of satisfying the first designing principle, an appropriate Xα should also make the apparent power of the converter as high as possible. In this way, the power capacity utilization rate of the compensating system can be increased.

In the typical variation range of load currents, the designed Xα should make the compensating system to have the obvious economic advantage than conventional RPC.

2) Designing Idea of Xα:

a) Realization of the first design principle: In order to meet the first designing principle, the second term of (5) seems to be an available method. Unfortunately, the load working condition in the real traction network is much complex, so that it is difficult to estimate.

Fig. 7 shows the phasor diagram of ALC-RPFC at four typical working conditions, in which, Icα, Icα', Icαm , and Icαm ' are the corresponded four compensating currents of conα, and satisfying Icα = Icα' < Icαm = Icαm '.Considering δα ∈ [30◦,90◦] (see Fig. 4), it can be deduced from Fig. 7 that 30◦ ≤ δαm ≤ δα ≤ 90.

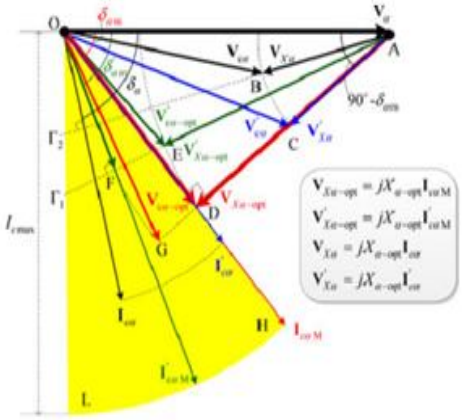

Fig. 7. Phasor diagram of ALC-RPFC in the variable load condition.

From Fig. 7, it can be concluded that, no matter how the railway load changes, all the compensating currents are located in the yellow fan-shaped area of OHL. Therefore, Icα and I cα' are the representative compensating currents of conα when their amplitudes is less than Icmax. While Icαm and Icαm are the representative ones when conα's

compensating currents is equal to Icmax. Besides, we must emphasize here that the load's PF is not a fixed value in both of those two cases; it changes the value along with δα. Additionally, when the compensating current equals Icmax, a suitable Xα should make conα operate at the minimal output voltage, e.g., OD and OF shown in Fig. 7. Because selecting the minimal output voltage as the normal voltage, a minimal apparent power can be obtained.

In the following, we will select an optimal one in those two representative cases:

1) If ΔADO is adopted to design Xα, it can be seen from Fig. 7 that when the compensating current changes from the normal current I cαm to another normal one Icαm ', the output voltage of conα will transform from OD to OE. Obviously OE < OD, which means, when the compensating current shifts along with arc HL, adopting ΔADO to design Xα, conα's output voltage will not exceed OD.

2) If ΔAFO is adopted to design Xα, similarly, when the compensating current changes from the normal current I cαm ' to another normal current Icαm , the output voltage of conα will transform from OF to OG. Hence, to get the minimal output voltage and apparent power of conα in the condition of load changes (i.e., the first design principle), select ΔADO to design Xα is better than others. From ΔADO, the optimal |Xα|, |Xα−opt|, can be calculated by

$$\left|X_{\alpha-opt}\right| = \frac{AD}{I_{c\alpha M}} = \frac{V_{X\alpha-opt}}{I_{c\alpha M}} = \frac{V_\alpha \sin\delta_{\alpha m}}{I_{c\alpha M}} \qquad (7)$$

where I cαm is the maximum value of Icα; δαm is the minimum compensating current angle of conα, and it satisfies [see (1)]

$$\delta_{\alpha m} = arctan\left(\frac{1}{\sqrt{3}} + 2\sqrt{\frac{1}{\lambda_{max}^2} - 1}\right) \qquad (8)$$

where λ max is the maximum PF of load current.

b) Verification of the second design principle: Referring to Fig. 7, when Icαm (normal current) decreases to Icα', ΔADO degenerates into ΔACO, and the output voltage of conα, however, increases from Vcα−opt (i.e., OD) to Vcα' (i.e., OC)

The terminal point of Vcα (point B) in ΔABO (the most ordinary working condition of conα) has to be constrained shifting in line AD, can the maximum value of S cα (the apparent power of conα) may be obtained. In this case, Icα → Icα', ΔABO→ΔACO.

From ΔACO, Scα can be calculated by

$$S_{c\alpha} = I_{c\alpha}V'_{c\alpha} = I_{c\alpha}\sqrt{V_\alpha^2 + I_{c\alpha}^2 X_{\alpha-opt}^2 - 2I_{c\alpha}\left|X_{\alpha-opt}\right|V_\alpha \sin\delta_{\alpha m}} \qquad (9)$$

Note that because ΔABOΔACO, Icα' is substituted by Icα in (9). Fig. 8 shows the relationship among Scα, Icα, and λmax, which is obtained by the per-unit expression of (9)

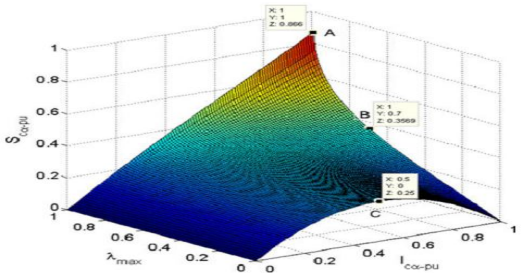

Fig. 8. Relationship among Scα , Icα , and λm ax (Note that the base values are selected as VB = Vα , IB = IcαM .).

2) Calculating Method of Xα−opt for Practical Application: Because I cα cannot be measured directly, (7) is not a convenient calculating method for practical application. The following, we will give a useful one for designing Xα−opt. The curve of ε(λ) is shown in Fig. 9 [originate from (3)]. Usually, the probability of locomotives' PF locates in 0.7~0.9 is much higher than other values. While, it can be observed from Fig. 9 that when λ ∈ [0.7,0.9], ε(λ) locates in a narrow interval of 0.8285~0.9808, which means Icα is approximately proportional with IL.

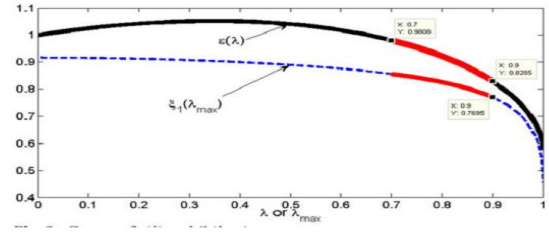

Fig. 9. Curves of ε(λ) and ξ1(λm ax).

So, referring to (2), Icαm can be approximately expressed as

$$I_{c\alpha M} \approx \frac{I_{LM}}{0.2}\int_{0.7}^{0.9}\varepsilon(\lambda)d\lambda = \varepsilon_{aver}I_{LM} = 0.916I_{LM} \qquad (10)$$

where ILM is the maximum value of IL, εaver is the average value of ε when λ ∈ [0.7,0.9].

Remark 1: For different electrical railway power system, the load's PF may not accurately distributes in 0.7~0.9, so it is better to modify εaver's value flexibly based on the form shown in (10), by applying the real statistic result of λ in practical applications. Substituting (10) and (8) into (7), the final practical used expression of |Xα−opt| can be expressed as

$$\left|X_{\alpha-opt}\right| = \frac{1}{\omega C_\alpha} - \omega L_\alpha = \xi_1\frac{V_\alpha}{I_{LM}} \qquad (11)$$

Where

$$\xi_1 = \varepsilon_{aver}\frac{\lambda_{max}/2\sqrt{3} + \sqrt{1-\lambda_{max}^2}}{-\sqrt{\frac{2}{3}\lambda_{max}^2 + \frac{\lambda_{max}}{\sqrt{3}}\sqrt{1-\lambda_{max}^2}+1}} \qquad (12)$$

For the consideration of designing convenience, the curve of ξ1(λmax) is also given in Fig. 9 (dotted line). The concept of 95%-probability

value is always be used in practical cases, so (11) can be also rewritten as

$$\left|X_{\alpha-opt}\right| = \frac{1}{\omega C_\alpha} - \omega L_\alpha = \xi_1 \left|\lambda_{max} = \lambda_{95\%(U)} \frac{V_\alpha}{I_{L-95\%(U)}}\right. \quad (13)$$

where λ 95%(U) and IL−95%(U) are the upper-95%-probability value of λ and IL, respectively.

Parameter Design of Phase-β

Fig. 10 shows the phasor diagram of phase-β, in which, ΔADO is the voltage triangle of conα, and it is the same with ΔADO shown in Fig. 7. IcβM is the maximum compensating current phasor of conβ, and it leads Vα 90°. VcβM is the maximum output voltage of conβ. Vβ lags Vα 60°.

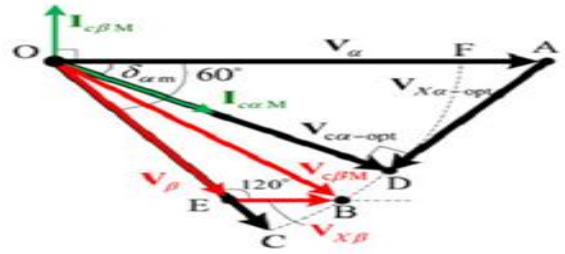

Fig. 10. Phasor diagram of phase-β.

In order to reduce the cost, improve the reliability of converters and design flexibility of the coupling branch, it is reasonable to make X β meet the following design principles:

1) It is better to make VcβM = Vcα−opt when the compensating current of conα reaches its maximum value Icαm .

2) In the premise of avoiding large inductance, designers should have sufficient flexibility to match the parameters of coupling branch when Vβ is a fixed value (it often happens in the renovation projects).

The typical voltage triangle of conβ in Fig. 10 is ΔBEO, where

$$\begin{cases} V_\beta = OE = \tau V_{c\alpha-opt}, 0 < \tau < 1 \\ V_{X\beta} = EB = \left|X_\beta\right| I_{c\beta M} \\ V_{c\beta M} = OB = OD = V_{c\alpha-opt} \end{cases} \quad (14)$$

in which EB is the voltage drop of the LC-coupling branch, Xβ is the fundamental reactance of the LC branch of phase-β. Besides, Vβ should be designed less than Vcα−opt (i.e., Vβ = τV cα−opt, 0 < τ < 1). Referring ΔADO in Fig. 10, and combine (14) and (7)–(12), it can be calculated that

$$V_\beta = \tau \sqrt{V_\alpha^2 - V_{X\alpha-opt}^2} = \frac{\tau \lambda_{max}}{2\sqrt{-\frac{2}{3}\lambda_{max}^2 + \frac{\lambda_{max}}{\sqrt{3}}\sqrt{1-\lambda_{max}^2}+1}} V_\alpha \quad (15)$$

Considering that when Icβ = IcβM , the active part of IL, I Lp(ILp = λIL), bound to reach its maximum value, so IcβM can be easily calculated by the current relationship shown in Fig. 3, i.e.

$$I_{c\alpha\beta M} = \frac{N}{2}\frac{I_{LM}\lambda_{max}}{\cos 30^0} = N\frac{I_{LM}\lambda_{max}}{\sqrt{3}} \quad (16)$$

where N = V α/Vβ. By using the cosine theorem in ΔBEO (see Fig. 10) and combining (14)–(16), |Xβ| can be calculated by

$$\left|X_\beta\right| = \frac{1}{\omega C_\beta} - \omega L_\beta = \xi_2 \frac{V_\alpha}{I_{LM}} \quad (17)$$

Where

$$\xi_2 = \frac{\sqrt{3\tau}\left(4-3\tau^2-\tau\right)cos^2\delta_{\alpha m}}{2\lambda_{max}}, 0 < \tau < 1 \quad (18)$$

Similar to design Xα, instead of λmax and ILM , λ95%(U) and IL−95%(U) can also be used in (15) and (17), (18) to calculate Vβ and X β in practical applications.

The design curve of Lβ and Cβ can be easily obtained from (17) and a real design example is shown in Fig. 17 of Section VI, which can be used to flexibly configure Lβ and Cβ according to the actual situation. For convenience of design, Fig. 11 gives the design surface of ξ2.

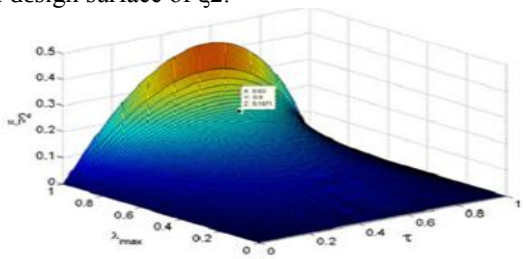

Fig. 11. Design surface of ξ2 .

Control System of Low-Rated Laboratory Model

Fig. 12 shows the control diagram of a low-rated ALC-RPFC. Based on the Fourier transformation theory, it can be verified that the output signal of low passive filter is ILp/√2 (ILp is the active part of IL) [17]. iα∗ and iβ ∗ are the expected output currents of T α and Tβ , respectively. For the consideration of resonance, when the control method shown in Fig. 12 is adopted, ALC-RPFC can be equivalent to an active filter with infinite harmonic damping factor in harmonic frequencies, so the harmonic resonance can be suppressed effectively

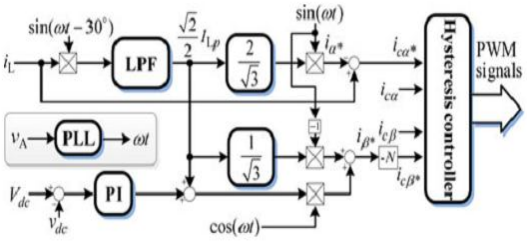

Fig. 12. Control diagram of low-rated ALC-RPFC

POWER CAPACITY ANALYSIS AND DC-LINK VOLTAGE DESIGN

For the same compensating task, ALC-RPFC and RPC have the same compensating currents, so the converters' power ratings of two systems are mainly decided by the output voltage of

conα [26], [27]. More accurately to say, is the dc-link voltage

Proposed ALC-RPFC

It can be observed from ΔACO in Fig. 7 that, when Icα' increases to I cαm,VX α' → VX α−opt, then conα's output volt age, Vcα', trends to its minimum value Vcα−opt. In addition, it can also be observed from ΔAEO of Fig. 7 that when I cαm → Icαm ',δαm → δαm ', which means the PF becomes smaller.

Conventional RPC

For RPC, the situation is reversed. It can be seen from Fig. 13 that, when Icα increases, the converter's output voltage VcαL of RPC (i.e., OB) will be much larger than Vα (i.e., OA). That is to say, the dc-link voltage of RPC has to be designed much higher than √2Vα .

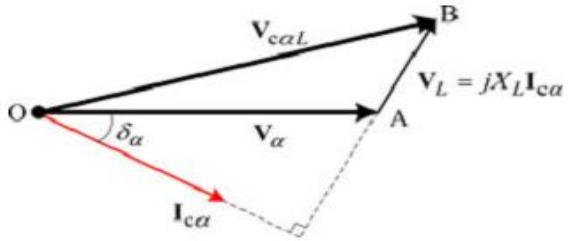

Fig. 13. Phasor diagram of RPC.

From Fig. 13, VcαL can be easily obtained from ΔABO, i.e.

$$V_{c\alpha L} = \sqrt{V_\alpha^2 + I_{c\alpha}^2 X_L^2 + 2I_{c\alpha} X_L V_\alpha \sin\delta_\alpha} \quad (19)$$

where XL is the reactance of the coupling inductance of RPC. Let XL = ξ|Xα−opt|, (ξ > 0), and considering (7), the perunit form of (19) can be calculated by

$$V_{c\alpha L-pu} = \sqrt{\left(\xi I_{c\alpha-pu} \sin\delta_{\alpha m}\right)^2 + 2\xi I_{c\alpha-pu} \sin\delta_{\alpha m} \sin\delta_\alpha + 1} \quad (20)$$

where the subscript "pu" represents the per-unit form of each variable. then ξ ∈ [0.45,0.55] (Section VI shows a practical designing example of Xα, in which |Xα−opt| = 46.9Ω). Let ξ = 0.5 and λmax = 0.9 (i.e., δαm = 57.1, because the probability of PF's upper-95%-probability value of locomotives distributes within 0.85~0.93 is much higher than other values), the 3-D plot of VcαL can be obtained from (20), and is shown in Fig. 14.

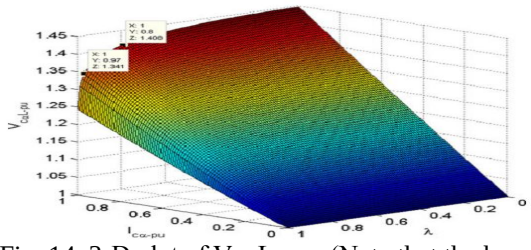

Fig. 14. 3-D plot of VcαL −pu (Note that the base values are VB = Vα , IB = IcαM .).

It can be seen from Fig. 14 that when λ = 0.8 (the typical PF of ac–dc locomotives) and Icα = 1.0 p.u., VcαL reaches its maximum value 1.408V α. So the dc-link voltage of RPC Vdc−L has to be designed to the peak value √2VcαL without consideration of harmonics compensation, i.e, Vdc−L ≈ 2Vα.

SIMULATION RESULT

The specifications of load currents adopted in the simulation are listed in Table I (measured data), in which, iLα1 and iLα2 are adopted to simulate the light (close to IL−95%(L)) and middle-load working conditions of the TSS, respectively.

Table I
Specifications Of Load Currents

	RMS/A	1th/A	3th/A	λ	THD%
$i_{\alpha L1}$	206.4	203.0	32.4	0.805	18.19
$i_{\alpha L2}$	314.4	312.7	57.0	0.746	20.57
$i_{\alpha L1} + i_{\alpha L2}$	524.3	514.9	89.4	0.812	19.16

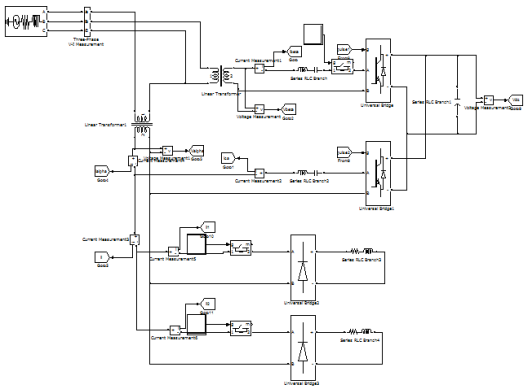

Fig.15 Block diagram of simulation.

Besides, iLα1 + iLα2 is adopted to simulate the heavy-load situation (close toIL−95%(U)). The simulating waveforms are shown in Figs. 16–21.

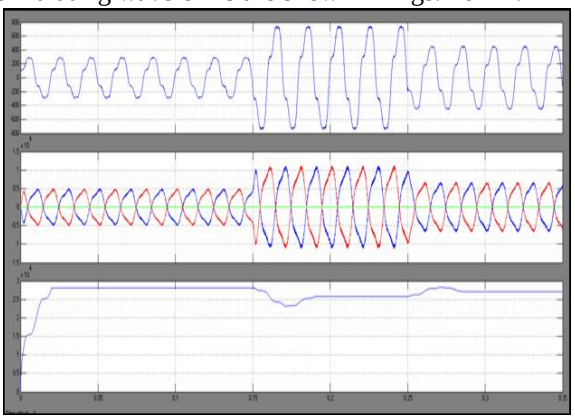

Fig. 16. Simulation waveforms without compensation. (a) Load currents. (b) Primary three phase currents. (c) Feeder voltage's RMS value of phase-α.

Compared with the uncompensated waveforms shown in Fig. 16, it can be observed from It validates the good compensating performance of RPC and ALC-RPFC; although the harmonic compensating performance of RPC is slightly worse than that of ALC-RPFC in the heavy-load case [see Fig. 17 (b)].

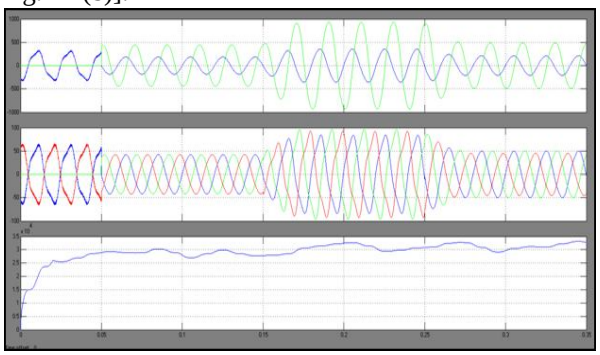

Fig. 17. Simulation waveforms of RPC system when Vdc-L = 66.7 kV. (a) Secondary output currents of main transformer. (b) Primary three phase currents. (c) Feeder voltage's RMS value of phase-α.

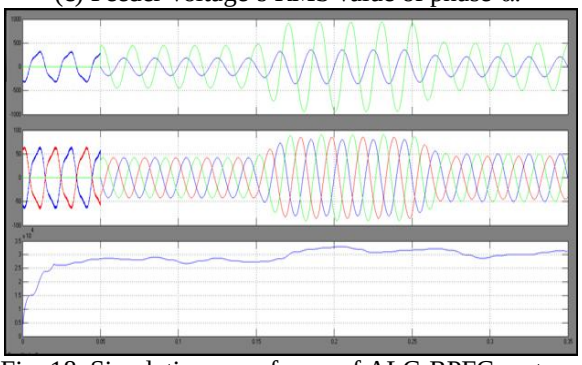

Fig. 18. Simulation waveforms of ALC-RPFC system when Vdc-LC = 38.9 kV. (a) Secondary output currents of main transformer. (b) Primary three phase currents. (c) Feeder voltage's RMS value of phase-α.

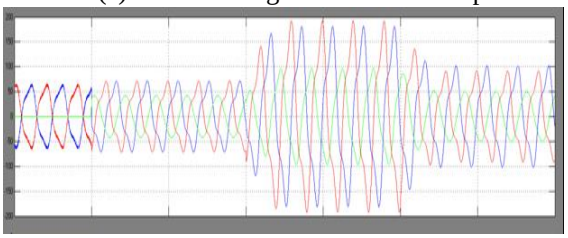

(a)

Fig. 19. Simulation waveforms of RPC and ALC-RPFC when the dc-link voltages decrease. (a) Primary three phase currents of RPC when Vdc-L = 58 kV.

It can be seen from Fig. 20(a) and (b) that, the conventional RPC shows a worse heavy-load compensating performance when Vdc-L decreases 13% (i.e., Vdc-L = 58 kV). However, when Vdc-LC decreases from 38.9 to 38.3 kV, ALC-RPFC's compensating performance is almost unchanged in heavy-load working condition [see Fig. 20(c) and (d)].

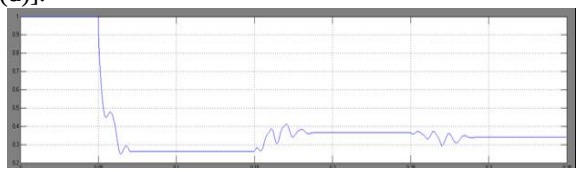

(b)

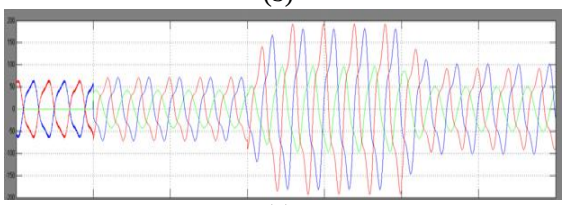

(c)

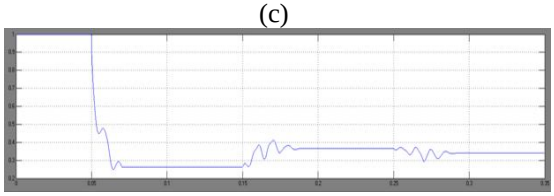

(d)

Fig. 20. Simulation waveforms of RPC and ALC-RPFC when the dc-link voltages decrease (b) Unbalance factor of primary three phase currents of RPC system when Vdc-L = 58 kV. (c) Primary three phase currents of ALC-RPFC when Vdc−LC = 38.3 kV. (d) Unbalance factor of primary three phase currents of ALC-RPFC system when Vdc-LC = 38.3 k

CONCLUSION

The proposed of an asymmetric double LC-coupled with railway power conditioner for a single-phase ac electric railway supply system is present in this paper. For the first time, its operating property undergoes the fluctuated load condition which is analyzed and explained in detailed. Therefore to reach the demand of applications form the "intense and random" load of the electrical railway power system, therefore here we are proposed a systematic design technique for LC-coupling branches, and also the power capacity analysis technique for the purpose of determining the design range of ALC-RPFC's dc-link voltage. At last the simulation results validate these conceptions. ALC-RPFC fully explores the potentials of two asymmetric passive LC branches. When comparison with the conventional RPC, it may have the excellent heavy-load compensating ability with lower dc-link voltage. Besides, all the parameters' design methods proposed in this paper are based on the fluctuated electrical railway working condition, and they are also useful for industrial applications. Therefore, the proposed conditioner is an industrial effective electric railway compensating system with high reliability and high cost-efficiency .

REFERENCES

[1] Z. He, H. Hu, Y. Zhang, and S. Gao, "Harmonic resonance assessment to traction power-supply system considering train model in china highspeed railway," IEEE Trans. Power Del., vol. 29, no. 4, pp. 1735–1743, Aug. 2014.
[2] S. L. Chen, R. J. Li, and H. Pao-Hsiang, "Traction system unbalance problem-analysis methodologies," IEEE Trans. Power Del., vol. 19, no. 4, pp. 1877–1883, Oct. 2004.
[3] E. Pilo de la Fuente, S. K. Mazumder, and I. Gonzalez Franco, "Railway electrical smart grids: An introduction to next-generation railway power systems and their operation," IEEE. Electrification Mag., vol. 2, no. 8, pp. 49–55, Sep. 2014. [4] T. Kneschke, "Control of utility system unbalance caused by single-phase electric traction," IEEE Trans. Ind. Appl., vol. IA-21, no. 6, pp. 1559–1570, Nov. 1985
[5] Z. Zhang, B. Wu, J. Kang, and L. Luo, "A multi-purpose balanced transformer for railway traction applications," IEEE Trans. Power Del., vol. 24, no. 2, pp. 711–718, Apr. 2009.
[6] H. Morimoto, T. Uzuka, A. Horiguchi, and T. Akita, "New type of feeding transformer for AC railway traction system," in Proc. Int. Power Electron. Drive Syst. Conf., 2009, pp. 800–805.
[7] S.V. Raygani, A. Tahavorgar, S.S. Fazel, and B. Moaveni, "Load flow analysis and future development study for an AC electric railway," IET Elect. Syst. Transportation, vol. 2, no. 3, pp. 139–147, Sep. 2012.
[8] X. He, Z. Shu, X. Peng, Q. Zhou, Y. Zhou, Q. J. Zhou, and S. Gao, "Advanced cophase traction power supply system based on three-phase to single-phase converter," IEEE Trans. Power Electron., vol. 29, no. 10, pp. 5323–5333, Oct. 2014
[9] S. Hu, Z. Zhang, Y. Li, L. Luo, Y. Cao, and C. Rehtanz, "A new halfbridge winding compensation based power conditioning system for electric railway with LQRI," IEEE Trans. Power Electron., vol. 29, no. 10, pp. 5242–5256, Oct. 2014.
[10] A.Bueno, J. Aller, J. Restrepo, R. Harley, and T. Habetler, "Harmonic and unbalance compensation based on direct power control for electric railway systems," IEEE Trans. Power Electron., vol. 28, no. 12, pp. 5823–5831, Dec. 2013.

M VENKATA SIVA

Completed B.Tech(Electrical &Electronics Engineering) from Alfa College of Engineering & Technology (Affiliated to J.N.T. University, Anantapur. Completed M.Tech, (Electrical &Electronics Engineering) from Siddharth Institute Of Engineering & Technology (Affiliated to J.N.T. University, Anantapur, Approved by A.I.C.T.E., New Delhi).

K. MANI

received B.Tech and M.Tech degrees in Electrical and Electronics Engineering from Jawaharlal Nehru Technological University, Hyderabad, India in 2007, and S.V.University, Tirupati, India in 2011 respectively. Currently he is pursuing Ph.D in S.V.University, Tirupati, and working as Associate Professor in Department of Electrical and Electronics Engineering, Siddharth Institute of Engineering & Technology, Puttur, India.